ARTICLE

OBC
www.rsc.org/obc

Methyl radical also reacts by the frontside mechanism: An *ab initio* study of some homolytic substitution reactions of methyl radical at silicon, germanium and tin †

Hiroshi Matsubara,*[a] Sonia M. Horvat[b] and Carl H. Schiesser*[b]

[a] *Department of Chemistry, Faculty of Arts and Sciences, Osaka Prefecture University, Sakai, Osaka 599-8531, Japan*

[b] *School of Chemistry, Bio21 Institute of Molecular Science and Biotechnology, The University of Melbourne, Victoria, 3010, Australia*

Received 18th November 2002, Accepted 30th January 2003
First published as an Advance Article on the web 4th March 2003

Ab initio calculations using 6-311G**, cc-pVDZ, aug-cc-pVDZ, and a (valence) double-ζ pseudopotential (DZP) basis sets, with (MP2, QCISD, CCSD(T)) and without (UHF) the inclusion of electron correlation, and density functional (B3LYP) calculations predict that homolytic substitution reactions of the methyl radical at the silicon atom in disilane can proceed *via* both backside and frontside attack mechanisms. At the highest level of theory (CCSD(T)/aug-cc-pVDZ//MP2/aug-cc-pVDZ), energy barriers ($\Delta E^{\ddagger}$) of 47.4 and 48.6 kJ mol^{-1} are calculated for the backside and frontside reactions respectively. Similar results are obtained for reactions involving germanium and tin with energy barriers ($\Delta E^{\ddagger}$) of between 46.5 and 67.3, and 41.0 and 73.3 kJ mol^{-1} for the backside and frontside mechanisms, respectively. These data suggest that homolytic substitution reactions of methyl radical at silicon, germanium, and tin can proceed *via* either homolytic substitution mechanism.

Introduction

Intermolecular free-radical substitution reactions, which are often referred to as homolytic substitution (S_H2) reactions, are now widely used in organic synthesis and have been well documented.[1,2] Work in our laboratories has been directed toward the design, application and understanding of free-radical homolytic substitution chemistry with the aim of developing novel synthetic methodology.[3] To that end, we published recently several *ab initio* studies with the aim of increasing our understanding of factors which affect and control the mechanism of homolytic substitution at several main-group higher heteroatoms. It is generally agreed that homolytic substitution reactions by an attacking radical (R) involves approach by the radical at the heteroatom (Y) along a trajectory opposite to the leaving group (Z). This *backside* mechanism can proceed either *via* a transition state **1** in which the attacking and leaving radicals adopt a collinear arrangement resulting in Walden inversion, or with the involvement of a hypervalent intermediate **2** which may or may not undergo pseudorotation prior to dissociation.[4] Indeed, high-level *ab initio* calculations support this view for reactions involving free radical attack at the pnicogens, chalcogens and halogens; reactions involving phosphorus[4,5] and tellurium[6] are predicted to involve intermediates, while sulfur,[6] selenium,[6] and the halogens[7] appear to proceed by direct displacement of the leaving group by a backside mechanism. †

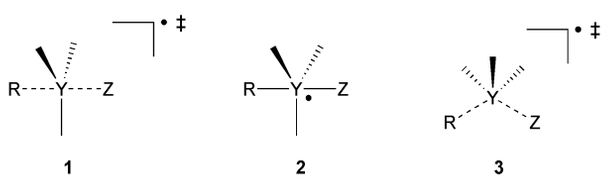

1 **2** **3**

In addition to the pathways for homolytic substitution described above, a mechanism involving *frontside* attack *via* transition state **3** has also recently been investigated. Indeed, Dobbs and Doren explored the mechanism of the reaction of a hydrogen atom with disilane and noted that frontside homolytic substitution is more favourable than the analogous backside mechanism by 11.7 kJ mol^{-1} at the MP2/6-311G** level of theory.[8] This value correlates well with available experimental data.[9] Similar computational investigations into the mechanism of the radical Brook rearrangement concluded that 1,2-migrations involving group (IV) elements proceed *via* frontside homolytic mechanisms.[10] The frontside attack pathway is also predicted in homolytic 1,2-translocation reactions between group (IV) elements,[11] while recent calculations suggest that both frontside and backside mechanisms have similar energy profiles for intermolecular degenerate homolytic substitution reactions involving silicon, germanium and tin.[12] In addition, only backside transition states are predicted to be involved in homolytic substitution reactions involving methyl radical at the heteroatom in methylsilane and methylgermane, whereas both backside and frontside transition states are predicted to be involved for the substitution of methyl radical at methylstannane.[12,13]

As part of an ongoing interest in homolytic substitution chemistry involving main group higher heteroatoms, and in order to explore the boundaries between frontside and backside mechanisms, we now report the results of computational investigations into the homolytic substitution mechanisms for reactions involving methyl radical at the heteroatom in disilane, digermane, distannane, silylgermane, silylstannane, and germylstannane.

Methods

Ab initio and DFT molecular orbital calculations were carried out on Compaq Personal Workstation 600au and Alpha Station DS10L computers using the Gaussian 98 program.[14] Geometry optimizations were performed using standard gradient techniques at the SCF, MP2, and B3LYP levels of theory using restricted (RHF, RMP2 and RB3LYP) and unrestricted (UHF, UMP2 and UB3LYP) methods for closed- and open-shell systems respectively.[15] All ground and transition states were verified by vibrational frequency analysis. Further single-point QCISD and CCSD(T) calculations were per-

† Electronic supplementary information (ESI) available: Optimized geometries and energies for the transition structures in this study. See http://www.rsc.org/suppdata/ob/b2/b211310d/

DOI: 10.1039/b211310d

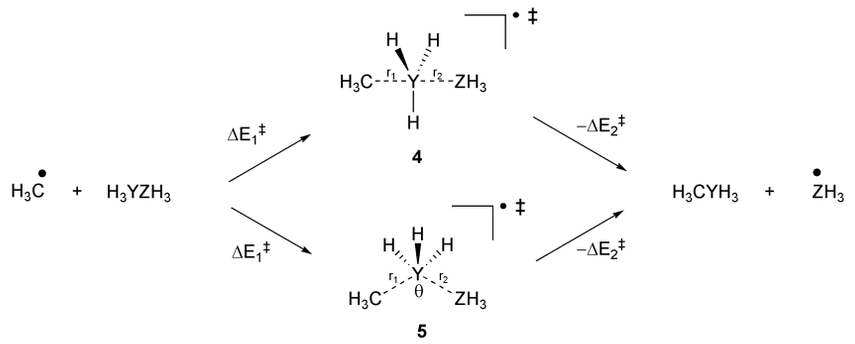

Scheme 1

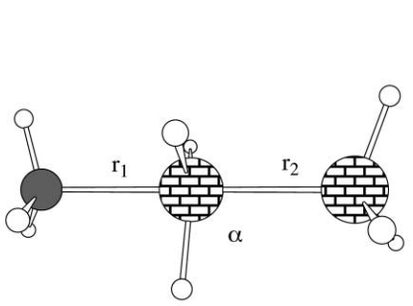

4

	r_1	r_2	α
UHF/6-311G**	2.179 Å	2.527 Å	90.6°
UHF/DZP	2.180 Å	2.525 Å	90.5°
MP2/6-311G**	2.208 Å	2.426 Å	95.1°
MP2/DZP	2.214 Å	2.426 Å	94.4°
MP2/cc-pVDZ	2.233 Å	2.450 Å	94.8°
MP2/aug-cc-pVDZ	2.240 Å	2.449 Å	95.0°
B3LYP/6-311G**	2.302 Å	2.441 Å	96.4°
B3LYP/DZP	2.282 Å	2.438 Å	95.7°

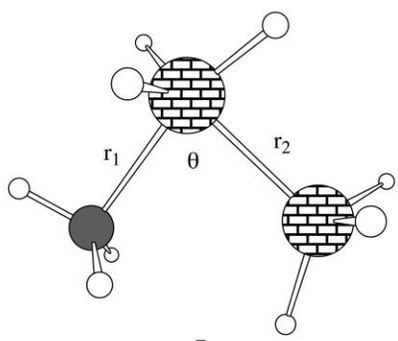

5

	r_1	r_2	θ
UHF/6-311G**	2.145 Å	2.523 Å	82.0°
UHF/DZP	2.129 Å	2.514 Å	82.4°
MP2/6-311G**	2.203 Å	2.403 Å	81.4°
MP2/DZP	2.177 Å	2.406 Å	79.0°
MP2/cc-pVDZ	2.225 Å	2.425 Å	82.1°
MP2/aug-cc-pVDZ	2.237 Å	2.429 Å	81.0°
B3LYP/6-311G**	2.248 Å	2.407 Å	85.6°
B3LYP/DZP	2.213 Å	2.392 Å	86.3°

Fig. 1 Optimized structures of transition state **4** and **5** (Y = Z = Si) for the backside and frontside substitution reactions of methyl radical with disilane.

formed on each of the MP2 optimized structures. When correlated methods were used, calculations were carried out using the frozen core approximation. Values of $<s^2>$ never exceeded 0.86 before annihilation of quartet contamination and were mostly 0.79 at correlated levels of theory. Where appropriate, zero-point vibrational energy (ZPE) corrections have been applied. Standard basis sets were used, as well as the (valence) double-ζ pseudopotential basis sets of Hay and Wadt[16] supplemented with a single set of *d*-type polarization functions for the heteroatoms in this study, (exponents $d(\zeta)_{Si} = 0.284$,[17] $d(\zeta)_{Ge} = 0.220$,[17] and $d(\zeta)_{Sn} = 0.200$), together with the double-ζ all-electron basis sets of Dunning[18] with an additional set of polarization functions (exponents $d(\zeta)_C = 0.75$ (Y = Z = Si) and $d(\zeta)_H = 1.00$) for C and H. We refer to this basis set as DZP throughout this work.[6,7,12] In previous work, results generated using DZP proved to be very similar to those obtained using 6-311G** for reactions involving chlorine and silicon.[10,12,13]

Optimized geometries and energies for all transition structures in this study (Gaussian Archive entries) are available as ESI.†

Results and discussion

Homolytic substitution reactions of methyl radical with disilane (Si_2H_6)

Extensive searching of the $H_3CYH_3ZH_3$ (Y = Z = Si) potential energy surfaces at the UHF/6-311G**, UHF/DZP, MP2/6-311G**, MP2/DZP, MP2/cc-pVDZ, MP2/aug-cc-pVDZ, B3LYP/6-311G**, and B3LYP/DZP levels of theory located hypervalent species **4** (Y = Z = Si), of C_{3v} symmetry, and **5** (Y = Z = Si), of C_1 symmetry, as transition states for the homolytic substitution of methyl radical at the silicon atom in disilane (Scheme 1).

In previous studies, we predicted that the $H_3ZYH_3ZH_3$ (Y, Z = Si, Ge, Sn) transition states **6** and **7** (Y, Z = Si, Ge, Sn), are involved in the degenerate homolytic substitution at silicon, germanium and tin.[12] However, in the study of $H_3CYH_3CH_3$ (Y = Si, Ge), only structure **6** (Y = Si, Ge; Z = C) involved in the backside attack mechanism for the degenerate methyl radical reactions was predicted, while both structures of **6** and **7** (Y = Sn, Z = C) corresponding backside and frontside attack mechanisms were calculated for tin-containing transition states.[12]

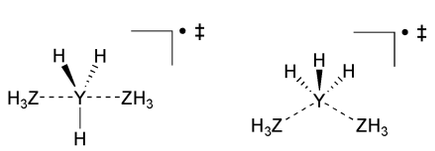

6 **7**

It is interesting to note that structures **4** (Y = Z = Si) and **5** (Y = Z = Si) involved in the backside and frontside mechanisms are predicted to exist as transition states for the homolytic substitution reaction of methyl radical with disilane. The important geometric features of the transition states **4** (Y = Z = Si) and **5** (Y = Z = Si) are summarized in Fig. 1, while calculated energy barriers ($\Delta E_1^{\ddagger}$ and $\Delta E_2^{\ddagger}$, Scheme 2) together with the corresponding imaginary frequencies are listed in Table 1. Full computational details are available as ESI.†

Table 1 Calculated energy barriers[a] for the forward ($\Delta E_1^{\ddagger}$) and reverse ($\Delta E_2^{\ddagger}$) homolytic substitution reactions of methyl radical to disilane (Si_2H_6) and imaginary frequencies (ν)[b] of transition states **4** and **5**

	4					**5**				
Method	$\Delta E_1^{\ddagger}$	$\Delta E_1^{\ddagger}$+ZPE	$\Delta E_2^{\ddagger}$	$\Delta E_2^{\ddagger}$+ZPE	ν	$\Delta E_1^{\ddagger}$	$\Delta E_1^{\ddagger}$+ZPE	$\Delta E_2^{\ddagger}$	$\Delta E_2^{\ddagger}$+ZPE	ν
UHF/6-311G**	133.4	144.3	168.7	168.7	1425i	134.7	148.6	170.0	173.0	628i
UHF/DZP	137.5	148.5	168.2	168.1	1351i	141.9	155.3	172.6	174.9	613i
MP2/6-311G**	65.8	75.3	139.8	140.1	910i	63.4	75.6	137.5	140.4	531i
MP2/DZP	69.7	79.8	127.8	128.4	889i	72.6	84.7	130.7	133.3	510i
MP2/cc-pVDZ	62.3	72.1	130.5	130.7	898i	63.6	75.3	131.8	134.0	527i
MP2/aug-cc-pVDZ	55.6	64.2	122.3	122.3	897i	53.5	64.4	120.1	122.6	512i
QCISD/6-311G**//MP2/6-311G**	65.2	—	125.8	—	—	65.8	—	126.4	—	—
QCISD/DZP//MP2/DZP	69.6	—	114.7	—	—	75.2	—	120.3	—	—
QCISD/cc-pVDZ//MP2/cc-pVDZ	63.1	—	118.0	—	—	67.1	—	122.1	—	—
QCISD/aug-cc-pVDZ// MP2/aug-cc-pVDZ	56.0	—	109.6	—	—	57.4	—	110.9	—	—
CCSD(T)/6-311G**//MP2/6-311G**	57.6	—	120.2	—	—	58.1	—	120.6	—	—
CCSD(T)/DZP//MP2/DZP	63.0	—	109.4	—	—	68.2	—	114.6	—	—
CCSD(T)/cc-pVDZ//MP2/cc-pVDZ	55.8	—	112.3	—	—	59.7	—	116.2	—	—
CCSD(T)/aug-cc-pVDZ// MP2/aug-cc-pVDZ	47.4	—	102.8	—	—	48.6	—	104.0	—	—
B3LYP/6-311G**	38.6	48.2	97.0	97.3	437i	46.9	57.5	105.2	106.5	327i
B3LYP/DZP	43.9	53.5	97.3	97.6	452i	52.1	62.6	105.5	106.6	322i

[a] Energies in kJ mol^{-1}. [b] Frequencies in cm^{-1}.

Table 2 UHF/DZP, MP2/DZP, and B3LYP/DZP calculated important geometric features of the transition structures **4** and **5**[a]

			4			**5**		
Y	Z	Method	r_1	r_2	α	r_1	r_2	θ
Si	Ge	UHF/DZP	2.202	2.598	90.9	2.165	2.596	81.2
		MP2/DZP	2.241	2.498	95.0	2.210	2.485	78.0
		B3LYP/DZP	2.328	2.506	96.6	2.246	2.483	80.9
Si	Sn	UHF/DZP	2.242	2.792	91.5	2.209	2.786	77.2
		MP2/DZP	2.286	2.682	95.8	2.272	2.656	76.8
		B3LYP/DZP	2.391	2.691	97.7	2.326	2.660	78.9
Ge	Si	UHF/DZP	2.267	2.643	89.6	2.226	2.659	78.6
		MP2/DZP	2.270	2.528	93.3	2.216	2.505	78.2
		B3LYP/DZP	2.315	2.547	94.0	2.213	2.499	86.2
Ge	Ge	UHF/DZP	2.288	2.715	89.9	2.255	2.735	78.3
		MP2/DZP	2.294	2.598	93.8	2.250	2.587	76.7
		B3LYP/DZP	2.357	2.611	95.1	2.277	2.577	83.7
Ge	Sn	UHF/DZP	2.321	2.904	90.5	2.285	2.924	75.3
		MP2/DZP	2.331	2.777	94.6	2.302	2.752	75.7
		B3LYP/DZP	2.413	2.789	96.4	2.336	2.760	78.5
Sn	Si	UHF/DZP	2.408	2.824	89.1	2.434	2.859	72.7
		MP2/DZP	2.390	2.709	92.5	2.377	2.728	72.1
		B3LYP/DZP	2.434	2.721	93.7	2.374	2.714	81.2
Sn	Ge	UHF/DZP	2.422	2.892	89.3	2.431	2.939	73.0
		MP2/DZP	2.406	2.778	92.8	2.408	2.791	71.9
		B3LYP/DZP	2.470	2.780	94.8	2.418	2.789	76.2
Sn	Sn	UHF/DZP	2.441	3.073	89.7	2.436	3.120	72.1
		MP2/DZP	2.431	2.952	93.5	2.454	2.945	71.5
		B3LYP/DZP	2.517	2.951	96.2	2.491	2.939	75.3

[a] Distances in Å and angles in degrees.

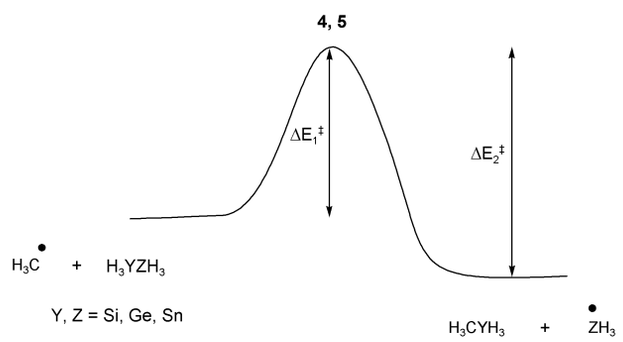

Scheme 2

Inspection of Fig. 1 reveals that while transition state **4** (Y = Z = Si) is predicted to adopt an exactly collinear arrangement (θ = 180°) of the attacking methyl radical and the leaving silyl radical at all levels of theory employed (C_{3v} symmetry), structure **5** (Y = Z = Si) involved in the analogous frontside chemistry is predicted to involve an attack angle (θ) of around 80° at all levels of theory; this angle is similar to those predicted for the frontside transition states involved in other homolytic substitution reactions involving silyl, germyl and stannyl radicals.[12] The transition state (Si–Si) separations in **4** (Y = Z = Si) and **5** (Y = Z = Si) are predicted at all levels of theory to lie in the range: 2.441 Å–2.527 Å and 2.392 Å–2.523 Å, respectively, while the (C–Si) distances in **4** (Y = Z = Si) and **5** (Y = Z = Si) are calculated to be 2.179 Å–2.302 Å, and 2.145 Å–2.248 Å, respectively. These distances are in the expected ranges when compared with our previous calculations.[10,12,13]

Not unexpectedly,[12] the data provided by this computational study suggests that the energy requirements for both homolytic pathways are similar. In addition, these reactions are predicted to be significantly exothermic at all level of theory. Inspection of Table 1 reveals that the energy barrier ($\Delta E_1^{\ddagger}$) for the forward reaction (Scheme 2) associated with **4** (Y = Z = Si) and **5** (Y = Z

Table 3 Calculated energy barriers[a] for the forward ($\Delta E_1^{\ddagger}$) and reverse ($\Delta E_2^{\ddagger}$) homolytic substitution reactions of methyl radical in **3** and transition state (imaginary) frequencies (ν)[b] of transition states **4** and **5**

			4					**5**				
Y	Z	Method	$\Delta E_1^{\ddagger}$	$\Delta E_1^{\ddagger}$+ZPE	$\Delta E_2^{\ddagger}$	$\Delta E_2^{\ddagger}$+ZPE	ν	$\Delta E_1^{\ddagger}$	$\Delta E_1^{\ddagger}$+ZPE	$\Delta E_2^{\ddagger}$	$\Delta E_2^{\ddagger}$+ZPE	ν
Si	Ge	UHF/DZP	127.6	138.5	176.6	175.3	1315i	133.3	146.8	182.3	183.7	609i
		MP2/DZP	62.8	72.8	142.1	141.4	856i	66.7	78.7	146.0	147.3	509i
		QCISD/DZP//MP2/DZP	61.7	—	128.8	—	—	68.5	—	135.6	—	—
		CCSD(T)/DZP//MP2/DZP	55.4	—	123.9	—	—	61.8	—	130.3	—	—
		B3LYP/DZP	37.3	46.7	110.7	109.8	439i	47.7	58.1	121.1	121.2	321i
Si	Sn	UHF/DZP	116.0	126.9	189.6	186.7	1226i	120.7	134.4	194.2	194.1	581i
		MP2/DZP	56.8	66.8	163.8	162.2	798i	57.6	70.1	164.5	165.5	486i
		QCISD/DZP//MP2/DZP	55.2	—	149.2	—	—	58.8	–	152.9	—	—
		CCSD(T)/DZP//MP2/DZP	49.3	—	145.6	—	—	52.7	–	149.0	—	—
		B3LYP/DZP	32.1	41.4	132.2	129.5	424i	40.5	51.6	140.6	139.6	327i
Ge	Si	UHF/DZP	142.2	152.2	152.7	152.2	1220i	145.8	158.2	156.2	158.1	548i
		MP2/DZP	75.1	84.6	117.0	117.5	868i	78.3	89.3	120.1	122.2	436i
		QCISD/DZP//MP2/DZP	74.2	—	103.5	—	—	80.6	—	109.9	—	—
		CCSD(T)/DZP//MP2/DZP	67.3	—	98.2	—	—	73.3	—	104.2	—	—
		B3LYP/DZP	48.0	57.1	84.4	84.7	417i	57.4	66.8	93.8	94.3	248i
Ge	Ge	UHF/DZP	131.7	141.7	158.6	156.9	1189i	135.9	148.3	162.9	163.5	527i
		MP2/DZP	67.6	77.1	128.3	127.6	843i	71.4	82.6	132.1	133.1	448i
		QCISD/DZP//MP2/DZP	65.9	—	114.6	—	—	72.9	—	121.5	—	—
		CCSD(T)/DZP//MP2/DZP	59.3	—	109.6	—	—	65.9	—	116.2	—	—
		B3LYP/DZP	40.4	49.6	94.9	94.0	402i	51.7	61.5	106.1	105.9	273i
Ge	Sn	UHF/DZP	120.7	130.9	167.5	164.3	1118i	124.3	136.8	171.1	170.3	501i
		MP2/DZP	61.3	70.9	145.2	143.8	791i	62.3	74.0	146.1	146.8	437i
		QCISD/DZP//MP2/DZP	59.0	—	130.1	—	—	63.2	—	134.3	—	—
		CCSD(T)/DZP//MP2/DZP	52.7	—	126.4	—	—	56.6	—	130.4	—	—
		B3LYP/DZP	35.0	44.0	111.8	109.3	393i	44.3	54.6	121.1	119.8	280i
Sn	Si	UHF/DZP	132.4	141.2	130.0	129.4	1415i	119.3	131.2	116.9	119.4	503i
		MP2/DZP	69.7	78.0	101.2	101.8	1036i	61.8	72.9	93.3	96.7	428i
		QCISD/DZP//MP2/DZP	65.5	—	83.7	—	—	61.9	—	80.1	—	—
		CCSD(T)/DZP//MP2/DZP	58.5	—	78.2	—	—	55.3	—	75.1	—	—
		B3LYP/DZP	33.6	42.0	61.0	61.6	366i	38.4	47.6	65.8	67.2	224i
Sn	Ge	UHF/DZP	124.8	133.6	134.0	132.4	1381i	112.1	123.8	121.3	122.5	478i
		MP2/DZP	64.1	72.4	110.1	109.5	1008i	55.7	66.6	101.7	103.7	428i
		QCISD/DZP//MP2/DZP	59.3	—	92.4	—	—	55.2	—	88.2	—	—
		CCSD(T)/DZP//MP2/DZP	52.5	—	87.3	—	—	48.8	—	83.6	—	—
		B3LYP/DZP	28.3	36.7	69.4	69.0	351i	32.8	42.9	73.9	75.2	218i
Sn	Sn	UHF/DZP	116.6	125.5	140.0	137.2	1293i	103.8	115.5	127.2	127.2	447i
		MP2/DZP	58.3	66.8	122.9	122.0	943i	47.9	59.0	112.4	114.1	409i
		QCISD/DZP//MP2/DZP	53.0	—	104.0	—	—	47.0	—	98.0	—	—
		CCSD(T)/DZP//MP2/DZP	46.5	—	100.2	—	—	41.0	—	94.7	—	—
		B3LYP/DZP	24.3	32.7	83.2	81.6	338i	27.1	37.4	86.1	86.2	224i

[a] Energies in kJ mol^{-1}. [b] Frequencies in cm^{-1}.

= Si) are calculated to be 133.4 and 134.7 kJ mol^{-1} respectively at the UHF/6-311G** level of theory. As expected, electron correlation is important in these calculations; MP2/ 6-311G** serves to lower these energy barriers to 65.8 and 63.4 kJ mol^{-1} for **4** (Y = Z = Si) and **5** (Y = Z = Si), respectively. Inclusion of zero-point vibrational energy correction (ZPE) serves to increase these barriers by about 10 kJ mol^{-1}. Further improvements in both basis set quality and levels of correlation provide values of $\Delta E_1^{\ddagger}$ for the reaction involving **4** (Y = Z = Si) that range from 55.6 (MP2/aug-cc-pVDZ) to 65.2 (QCISD/6-311G**//MP2/6-311G**). In comparison, reactions involving **5** (Y = Z = Si) are calculated to have values of $\Delta E_1^{\ddagger}$ in the range: 53.5 (MP2/aug-cc-pVDZ) to 65.8 (QCISD/6-311G**//MP2/6-311G**). At the highest level of theory used (CCSD(T)/aug-cc-pVDZ//MP2/aug-cc-pVDZ), energy barriers ($\Delta E_1^{\ddagger}$) of 47.4 (Y = Z = Si) and 48.6 kJ mol^{-1} are predicted for the reaction involving **4** (Y = Z = Si) and **5** (Y = Z = Si), respectively, while values 38.6 (Y = Z = Si) and 46.9 kJ mol^{-1} are obtained at the B3LYP/6-311G** level of theory. As the difference between the two pathways involving **4** (Y = Z = Si) and **5** (Y = Z = Si) is calculated to be only 1.2 kJ mol^{-1} at the highest level of theory, we conclude that homolytic substitution by a methyl radical at disilane can proceed by either backside or frontside mechanism.

As we have noted on other occasions, the B3LYP method provides data that can be different enough to those provided using other methods to deserve mention.[11,12,19] In particular (Table 1) the B3LYP/6-311G** method predicts a difference of some 8 kJ mol^{-1} in the barriers ($\Delta E_1^{\ddagger}$) for the attack of methyl radical at disilane by the backside and frontside mechanisms respectively; suggesting that the backside mechanism is favoured and contradicting the other methods employed.

Homolytic substitution reaction of methyl radical with digermane (Ge_2H_6), distannane (Sn_2H_6), silylgermane (H_3SiGeH_3), silylstannane (H_3SiSnH_3), and germylstannane (H_3GeSnH_3)

Extensive searching of the $H_3CYH_3ZH_3$ (Y, Z = Si, Ge, Sn) potential energy surfaces at the UHF/DZP, MP2/DZP, and B3LYP/DZP levels of theory located transition states **4** (Y, Z = Si, Ge, Sn) and **5** (Y, Z = Si, Ge, Sn). The important geometric features of these structures are shown in Table 2 and the calculated energy barriers ($\Delta E_1^{\ddagger}$, $\Delta E_2^{\ddagger}$) for the forward and reverse reactions respectively) are listed in Table 3. Full structural details are available as ESI. †

The structures in Table 2 bear a striking resemblance to the those calculated for the analogous reactions with disilane **4** (Y = Z = Si) and **5** (Y = Z = Si). Backside attack structures **4** (Y = Z = Si) are predicted to adopt a collinear arrangement of attacking and leaving radicals, while the frontside structures **5** (Y = Z = Si) are calculated to have angles (θ) of about 71–86° between attacking and leaving species. The size of the attack angle decreases in progressing from silicon to germanium and

tin. For example, angle (θ) in **5** (Y = Si, Z = Ge) is predicted to be 78.0° at the MP2/DZP level of theory, slightly larger than that in **5** (Y = Si, Z = Sn): 76.8°, **5** (Y = Z = Ge): 76.7°, **5** (Y = Sn, Z = Si): 72.1°, and **5** (Y = Z = Sn): 71.5°. The hydrogen atoms on the central heteroatom (Y) in structure **4** involved in the backside mechanism are predicted to slightly incline toward the methyl group at all correlated levels of theory, consistent with an "early" transition state in the direction indicated in Scheme 1.

As can be seen in Table 2, C–Y distances (r_1) in **5** are calculated to lie between 2.210 (Y = Si, Z = Ge) and 2.454 Å (Y = Z = Sn) at the MP2/DZP level of theory, while Y–Z separations (r_2) in **5** are predicted to be in the range: 2.485 (Y = Si, Z = Ge)–2.945 Å (Y = Z = Sn). Similar trends are also observed for **4**, the transition stated involved in the frontside mechanism at the MP2/DZP level of theory. Interestingly, it should be noted that B3LYP calculations predict structures for **4** and **5** with larger angles and greater separations than those calculated using more traditional methods.

Inspection of Table 3 reveals that some interesting trends in energy are clearly evident. As can be seen in the table, calculated energy barriers ($\Delta E_2^{\ddagger}$) for the reverse reactions (Scheme 2) are always larger than those ($\Delta E_1^{\ddagger}$) for the forward process at all level of theory; these reactions are predicted to be exothermic at all levels of theory. Calculated energy barriers ($\Delta E^{\ddagger}$) are also affected strongly by the inclusion of electron correlation. At any given level of theory, the values of $\Delta E_1^{\ddagger}$ and $\Delta E_2^{\ddagger}$ are clearly dependent on the nature of atom undergoing homolytic substitution and the leaving radical. As observed in previous work, for given attacking and leaving radicals involved at the group (IV) heteroatom, the order of reactivity is usually: Sn > Si ≥ Ge.[12] It is noteworthy that the results obtained in this work reveal the same trend, namely that the order of reactivity for attack of methyl radical at a group (IV) heteroatom with the same leaving group is: Sn > Si > Ge. For example, at the highest level of theory (CCSD(T)/DZP//MP2/DZP) values of 67.3 and 58.5 kJ mol^{-1} are calculated for the backside attack of methyl radical at the germanium and tin atoms in silylgermane and silylstannane (germyl and stannyl radical as leaving groups), respectively. These numbers are to be compared with the value of 63.0 kJ mol^{-1} (Table 1) for the analogous reaction with disilane at the same level of theory. The similar data for the analogous frontside reactions are 68.2 (Si), 73.3 (Ge), and 55.3 kJ mol^{-1} (Sn). On the other hand, the energy barriers for reactions involving **4** (Y = Si) are predicted to be 63.0 (Z = Si), 55.4 (Z = Ge), and 49.3 kJ mol^{-1} (Z = Sn) at the highest level of theory; similar data are obtained for the analogous reactions involving **5**.

Importantly, the computational data presented in this work indicate that both frontside and backside attack mechanism are predicted to be feasible at all levels of theory employed. For example, at the CCSD(T)/DZP//MP2/DZP level of theory, the backside reaction is favoured over the reaction involving **5** by 3.4–6.4 kJ mol^{-1} for attack at silicon and by 3.9–6.6 kJ mol^{-1} for attack at germanium. However, the frontside mechanism is predicted to be favoured slightly for reactions involving attack at tin at all levels of theory (except B3LYP/ZDP); CCSD(T)/DZP//MP2/DZP calculations predict that the frontside process involving tin is favoured by 3.2 kJ mol^{-1} (Z = Si), 3.7 kJ mol^{-1} (Z = Ge) and 5.5 kJ mol^{-1} (Z = Sn).

Acknowledgements

We gratefully acknowledge the support of the Melbourne Advanced Research Computing Centre.

References

1 For leading reviews, see: J. C. Walton, *Acc. Chem. Res.*, 1998, **31**, 99; C. H. Schiesser and L. M. Wild, *Tetrahedron*, 1996, **52**, 13265; J.-M. Saveant, *Tetrahedron*, 1994, **50**, 10117; A. L. J. Beckwith, *Chem. Soc. Rev.*, 1993, **22**, 143; R. A. Rossi and S. M. Palacios, *Tetrahedron*, 1993, **49**, 4485.

2 For some recent reports, see: C. A. G. Carter, G. Greidanus, J.-X. Chen and J. M. Stryker, *J. Am. Chem. Soc.*, 2001, **123**, 8872; A. M. Stolzenberg and Y. Cao, *J. Am. Chem. Soc.*, 2001, **123**, 9078; S. E. Tichy, K. K. Thoen, J. M. Price, J. J. Ferra, Jr., C. J. Petucci and H. I. Kenttaemaa, *J. Org. Chem.*, 2001, **66**, 2726; N. Al-Maharik, L. Engman, J. Malmström and C. H. Schiesser, *J. Org. Chem.*, 2001, **66**, 6286; S.-K. Kang, H.-W. Seo and Y.-H. Ha, *Synthesis*, 2001, 1321; M.-J. Bourgeois, M. Vialemaringe, M. Campagnole and E. Mountaudon, *Can. J. Chem.*, 2001, **79**, 257; M. W. Carland, L. R. Martin and C. H. Schiesser, *Tetrahedron Lett.*, 2001, **42**, 4737; J. B. Miller and J. R. Salvador, *J. Org. Chem.*, 2002, **67**, 435; P. Lightfoot, P. Pareschi and J. C. Walton, *J. Chem. Soc., Perkin Trans. 2*, 2002, 918; L. Benati, R. Leardini, M. Minozzi, D. Nanni, P. Spagnolo, S. Strazzari and G. Zanardi, *Org. Lett.*, 2002, **4**, 3079; J. Hartung, T. Gottwald and K. Spehar, *Synthesis*, 2002, 1469.

3 C. H. Schiesser and K. Sutej, *Tetrahedron Lett.*, 1992, **33**, 5137; J. E. Lyons, C. H. Schiesser and K. Sutej, *J. Org. Chem.*, 1993, **58**, 5632; L. J. Benjamin, C. H. Schiesser and K. Sutej, *Tetrahedron*, 1993, **49**, 2557; M. C. Fong and C. H. Schiesser, *Tetrahedron Lett.*, 1995, **36**, 7329; M. A. Lucas and C. H. Schiesser, *J. Org. Chem.*, 1996, **61**, 5754; M. C. Fong and C. H. Schiesser, *J. Org. Chem.*, 1997, **62**, 3103; M. J. Laws and C. H. Schiesser, *Tetrahedron Lett.*, 1997, **38**, 8429; M. A. Lucas and C. H. Schiesser, *J. Org. Chem.*, 1998, **63**, 3032; L. Engman, M. J. Laws, J. Malmström, C. H. Schiesser and L. M. Zugaro, *J. Org. Chem.*, 1999, **64**, 6764; M. A. Lucas, O. T. K. Nguyen, C. H. Schiesser and S.-L. Zheng, *Tetrahedron*, 2000, **56**, 3995.

4 C. H. Schiesser and L. M. Wild, *Aust. J. Chem.*, 1995, **48**, 175.

5 J. M. Howell and J. F. Olsen, *J. Am. Chem. Soc.*, 1976, **98**, 7119; C. J. Cramer, *J. Am. Chem. Soc.*, 1990, **112**, 7965; C. J. Cramer, *J. Am. Chem. Soc.*, 1991, **113**, 2439.

6 K. F. Ferris, J. A. Franz, C. Sosa and R. J. Bartlett, *J. Org. Chem.*, 1992, **57**, 777; J. E. Lyons and C. H. Schiesser, *J. Chem. Soc., Perkin Trans. 2*, 1992, 1655; J. E. Lyons and C. H. Schiesser, *J. Organomet. Chem.*, 1992, **437**, 165; B. A. Smart and C. H. Schiesser, *J. Chem. Soc., Perkin Trans. 2*, 1994, 2269; C. H. Schiesser and B. A. Smart, *Tetrahedron*, 1995, **51**, 6051; C. H. Schiesser, B. A. Smart and T.-A. Tran, *Tetrahedron*, 1995, **51**, 10651; C. H. Schiesser and B. A. Smart, *J. Comput. Chem.*, 1995, **16**, 1055; C. H. Schiesser and M. A. Skidmore, *Chem. Commun.*, 1996, 1419; C. H. Schiesser and M. A. Skidmore, *J. Organomet. Chem.*, 1998, **552**, 145; C. H. Schiesser and L. M. Wild, *J. Org. Chem.*, 1999, **64**, 1131.

7 C. H. Schiesser, B. A. Smart and T.-A. Tran, *Tetrahedron*, 1995, **51**, 3327; C. H. Schiesser and L. M. Wild, *J. Org. Chem.*, 1998, **63**, 670.

8 K. D. Dobbs and D. J. Doren, *J. Am. Chem. Soc.*, 1993, **115**, 3731.

9 L. Fabry, P. Potzinger, B. Reinmann, A. Ritter and H. P. Steenberger, *Organometallics*, 1986, **5**, 1231.

10 C. H. Schiesser and M. L. Styles, *J. Chem. Soc., Perkin Trans. 2*, 1997, 2335.

11 S. M. Horvat and C. H. Schiesser, *J. Chem. Soc., Perkin Trans. 2*, 2001, 939.

12 S. M. Horvat, C. H. Schiesser and L. M. Wild, *Organometallics*, 2000, **19**, 1239.

13 C. H. Schiesser, M. L. Styles and L. M. Wild, *J. Chem. Soc., Perkin Trans. 2*, 1996, 2257.

14 *Gaussian 98, Revision A.7*, M. J. Frisch, G. W. Trucks, H. B. Schlegel, G. E. Scuseria, M. A. Robb, J. R. Cheeseman, V. G. Zakrzewski, J. A. Montgomery, Jr., R. E. Stratmann, J. C. Burant, S. Dapprich, J. M. Millam, A. D. Daniels, K. N. Kudin, M. C. Strain, O. Farkas, J. Tomasi, V. Barone, M. Cossi, R. Cammi, B. Mennucci, C. Pomelli, C. Adamo, S. Clifford, J. Ochterski, G. A. Petersson, P. Y. Ayala, Q. Cui, K. Morokuma, D. K. Malick, A. D. Rabuck, K. Raghavachari, J. B. Foresman, J. Cioslowski, J. V. Ortiz, A. G. Baboul, B. B. Stefanov, G. Liu, A. Liashenko, P. Piskorz, I. Komaromi, R. Gomperts, R. L. Martin, D. J. Fox, T. Keith, M. A. Al-Laham, C. Y. Peng, A. Nanayakkara, C. Gonzalez, M. Challacombe, P. M. W. Gill, B. Johnson, W. Chen, M. W. Wong, J. L. Andres, C. Gonzalez, M. Head-Gordon, E. S. Replogle and J. A. Pople, Gaussian, Inc., Pittsburgh PA, 1998.

15 W. J. Hehre, L. Radom, P. v. R. Schleyer and P. A. Pople, *Ab Initio Molecular Orbital Theory*, Wiley, New York, 1986.

16 W. R. Wadt and P. J. Hay, *J. Chem. Phys.*, 1985, **82**, 284; P. J. Hay and W. R. Wadt, *J. Chem. Phys.*, 1985, **82**, 270; P. J. Hay and W. R. Wadt, *J. Chem. Phys.*, 1985, **82**, 299.

17 A. Höllwarth, M. Böhme, S. Dapprich, A. W. Ehlers, A. Gobbi, V. Jonas, K. F. Köhler, R. Stegmann, A. Veldkamp and G. Frenking, *Chem. Phys. Lett.*, 1993, **208**, 237.

18 T. H. Dunning and P. J. Hay, *Modern Theoretical Chemistry*, Plenum, New York, 1976, ch. 1, pp. 1–28.

19 T. Morihovitis, C. H. Schiesser and M. A. Skidmore, *J. Chem. Soc., Perkin Trans. 2*, 1999, 2041.